Nanoscale

PAPER

View Article Online
View Journal | View Issue



Cite this: *Nanoscale*, 2020, **12**, 7051

# Dual photothermal MDSCs-targeted immunotherapy inhibits lung immunosuppressive metastasis by enhancing T-cell recruitment†

Kalliopi Domvri,[a] Savvas Petanidis, *[b,c] Doxakis Anestakis,[b,c,d] Konstantinos Porpodis,[a] Chong Bai,[e] Paul Zarogoulidis,[f] Lutz Freitag,[g] Wolfgang Hohenforst-Schmidt[h] and Theodora Katopodi[b]

Immunosuppressive chemoresistance is a major barrier in lung cancer treatment. However, the immunosuppressive mechanisms responsible for lung cancer cell chemoresistance and tumor relapse are still unknown. In this study, we introduce a model of precise immunosuppressive-based nanotherapy by designing and delivering biocompatible MDSC-targeted nanocarriers (NCs) into the lung tumor microenvironment. This is accomplished by conjugating L-Norvaline and Sunitinib integrated into biodegradable nanosomes in order to facilitate inhibition of tumor-supporting immunosuppression. Findings show that treatment with NCs increased apoptosis and significantly reduced tumor volume and Ki-67 antigen expression respectively. Biodistribution analysis revealed an increase in drug circulation time, as well as a greater accumulation in lung and peripheral tissues. Furthermore, an upregulation of tumor infiltrating lymphocytes expression was observed, especially $CD8^+$ T cells by 27%, and $CD4^+$ T cells by 7% compared to PBS treatment. The presence of $CD161^+$ (NK1.1) cells revealed NK cell activation followed by decreased MDSC infiltration and MDSC subsets were characterized by the reduction of Gr/CD11b cell population in blood and tissue samples. In addition, these nanospheres, showed increased PTT efficiency and tumour targeting ability as evidenced by highly efficient tumour ablation under near infrared (NIR) exposure. Significant tumor reduction was observed due to recruitment of cytotoxic T-lymphocytes, followed by downregulation of immunosuppressive $Foxp3^+$ Treg cells. Taken together, our findings provide a novel nanodrug delivery strategy for the inhibition of MDSC-related immunosuppression in lung tumor microenvironment and provide a new approach for the efficient treatment of metastatic cancer.

Received 4th January 2020,
Accepted 9th March 2020

DOI: 10.1039/d0nr00080a

rsc.li/nanoscale



## Introduction

Lung cancer remains the leading cause of cancer-related deaths and despite extensive research efforts, the survival rate of lung cancer patients remains significantly low.[1,2] Immunotherapy strategies against lung neoplasia aims at the induction and subsequent migration of tumor-antigen specific T cells into the tumor.[3,4] These approaches generate both tumor antigen-specific T cells and trigger the intratumoral infiltration of T cells.[5,6] However, immunosuppressive cells present in the tumor microenvironment can restrain the action of tumor antigen-specific T cells and impede immune-based tumor eradication.[7,8]

Myeloid-derived suppressor cells (MDSCs) are immunosuppressive cells of myeloid origin composed of immature macrophages, granulocytes and dendritic cells.[9] MDSCs can be subdivided into two major groups: granulocytic MDSC (gMDSC) and monocytic MDSC (mMDSC). The gMDSCs have a morphology similar to that of granulocytes, whereas mMDSCs have

[a]*Pulmonary Department-Oncology Unit, "G. Papanikolaou" General Hospital, Aristotle University of Thessaloniki, Thessaloniki, 57010, Greece*
[b]*Department of Medicine, Laboratory of Medical Biology and Genetics, Aristotle University of Thessaloniki, Thessaloniki, 54124, Greece. E-mail: spetanid@auth.gr; Fax: +30-2310-999-228; Tel: +30-2310-999-225*
[c]*Department of Pulmonology, I.M. Sechenov First Moscow State Medical University, Moscow, 119992, Russian Federation*
[d]*Department of Medicine, Laboratory of Forensic Medicine and Toxicology, Aristotle University of Thessaloniki, 54124, Greece*
[e]*Department of Respiratory & Critical Care Medicine, Changhai Hospital, Second Military Medical University, Shanghai, 200433, China*
[f]*Third Department of Surgery, "AHEPA" University Hospital, Aristotle University of Thessaloniki, 55236 Thessaloniki, Greece*
[g]*Department of Pulmonology, University Hospital Zurich, Rämistrasse 100, 8091 Zurich, Switzerland*
[h]*Medical Clinic I, 'Fuerth' Hospital, University of Erlangen, 91054 Fuerth, Germany*
†Electronic supplementary information (ESI) available. See DOI: 10.1039/d0nr00080a

a morphology similar to that of monocytes.[10] Increased levels of MDSCs have been reported in spleen, bone marrow and circulation in tumor-bearing animals and cancer patients.[11] Intratumoral MDSC levels correlate with tumor progression, metastasis and resistance to cancer therapies.[12] In mice, MDSCs are identified by the simultaneous expression of the myeloid antigens CD11b and Gr-1 on their cell membrane. MDSCs can suppress T-cell functions *via* inducible nitric oxide synthase (iNOS) and arginase-1 (ARG1).[13,14] To overcome the immunosuppressive effects of MDSCs and potentiate antitumoral immune responses, depletion or functional inhibition of MDSCs in combination with immunization regimens could be a beneficial approach.[15,16]

Sunitinib is a receptor tyrosine kinase inhibitor (TKI) that is front-line therapy for metastatic renal cell carcinoma (mRCC).[17] Its antitumor activity is related to its ability to block tumor cell and tumor vasculature cell signaling *via* several TKI receptors, like vascular endothelial growth factor receptors VEGFRs, platelet-derived growth factors (PDGFs), stem cell factors.[18] Sunitinib also targets myeloid derived suppressor cells (MDSCs) significantly reducing their accumulation in the peripheral blood and reversing T cell suppression in both mRCC patients and in murine tumor models.[19] The simultaneous inhibition of these targets therefore reduces tumor vascularization and triggers neoplastic cell apoptosis and thus results in tumor shrinkage.[20] In a similar manner, Norvaline is an arginase inhibitor that has been reported to rectify T cell subpopulations like Tregs, Th17, γδT and Tregs/Th17 restoring immune imbalance.[21,22] The combined use of L-Norvaline and Sunitinib is able to inhibit MDSC-derived tumor immunosuppression by depleting the MDSC subset populations in the lung tumor microenvironment and reactivating the immune mechanism.

On this basis we have developed a specialized nano-platform, composed of copper sulfide nanocarriers (CuS NCs) that enclose the Norvaline/Sunitinib (NorSun) prodrug complexes for "photothermal immunotherapy" targeting of MDSCs in a mouse lung cancer model. After laser excitation, these complexes break down, reassemble, and transform into polymer complexes that enhance tumor retention and represent an immunostimulatory dual-functional nanocarrier that facilitates co-delivery of chemotherapeutics and improves cancer immunochemotherapy. Results reveal that treatment with NCs increases TUNEL-related apoptosis and significantly reduces tumor volume and Ki-67 antigen expression respectively. Furthermore, tumor infiltrating lymphocytes expression was observed, especially $CD8^+$ T cells and $CD4^+$ T cells followed by upregulation of $CD161^+$ NK cells. This NK cell activation prompted decreased MDSC infiltration and most MDSC subsets were characterized by the reduction of Gr/CD11b cell population in blood and tissue samples. In addition, these nanospheres, showed increased PTT efficiency and tumour targeting ability as evidenced by highly efficient tumour ablation under near infrared (NIR) exposure. Significant tumor reduction was observed due to recruitment of cytotoxic T-lymphocytes, followed by downregulation of immunosuppressive $Foxp3^+$ Treg cells. The CuS/NorSun-mediated photothermal therapy, exhibited potent innate and adaptive immune response, resulting in combined antitumor effects against primary and secondary tumors. These CuS/NorSun NCs are biodegradable and can be eliminated from the body after laser irradiation causing depletion or functional inactivation of the immunosuppressive MDSC population. Overall, these findings demonstrate the crucial role of MDSC-targeted nanoplatform in inhibiting lung immunosuppression and provide new opportunities for the effective inhibition of metastatic neoplasia.

# Methods

### Ethics statement

The study was approved by the local Ethics Committee on human experimentation of the AHEPA Hospital, Medical School, Aristotle University of Thessaloniki and informed consent was obtained from each patient before the surgical procedure.

### Synthesis of CuS/NorSun NCs

For the synthesis of CuS NPs, 1000 mL of an aqueous solution of $CuCl_2$ (1 mmol) and sodium citrate (0.68 mmol) was added 1 mL of sodium sulfide solution ($Na_2S$, 1 M) under stirring at room temperature. Five minutes later, the reaction mixture was heated to 90 °C and stirred at 1000 rpm for 4 h until a dark green solution was obtained. Nanoparticles with peak absorption at 980 nm were obtained by adjusting the stoichiometric ratio between $CuCl_2$ and $Na_2S$. Next, isolated CuS (30 mg) were dispersed into 100 ml of PLGA-PEG-3000 ($M_w$ = 3000) in ethanol solution (0.5 mg $ml^{-1}$) and magnetic stirring was applied at 50 °C. After 12 h of PEGylation process, the CuS NCs were centrifuged and rinsed with ethanol and $ddH_2O$ to remove the residual PEG. The obtained PEGylated CuS NCs were dissolved into 10 ml of sodium acetate buffer (2 M) under mild magnetic stirring, followed by the addition of norvaline (10 mg) and sunitinib (10 mg). After 24 h, the resulting CuS/NorSun NCs were obtained by centrifugation, dispersed in PBS (pH 7.4) and stored at 4 °C.

### Conjugation of Rhodamine B isothiocyanate on CuS/NorSun NCs

Five ml of isolated CuS/NorSun NCs NPs were centrifuged and redispersed in 10 mL of MES buffer (20 mM, pH 6.0). Next, RHB isothiocyanate was added to the mixture and gently stirred for 24 h in the dark at room temperature. Then, particles were repeatedly washed with distilled water several times to remove redundant Rhodamine B.

### *Ex vivo* tissue culture

Lung tumor samples from consenting lung cancer (KRAS, chemoresistant) patients at the AHEPA Hospital Oncology unit were collected, transferred to research lab in cold media, and processed in a sterile tissue culture hood (ESI†). The culture protocol is modified based on previous studies.[23,24] Briefly, the

 

culture medium consists of Dulbecco's modified Eagle's medium supplemented with 5% fetal calf serum (FCS), 10 mM HEPES, 0.5 μg $ml^{-1}$ hydrocortisone, 1% MEM vitamins solution, 5 μg $ml^{-1}$ insulin, 100 IU $ml^{-1}$ penicillin, 100 μg $ml^{-1}$ streptomycin, and 15 μg $ml^{-1}$ gentamicin. The tissue is placed in a sterile glass dish where all necrotic and visible connective tissue is removed. Tissue samples are cut in 0.5 $cm^3$ to 1.0 $cm^3$ slices *via* a cryotome and placed in a 6-well tissue culture dish with 2 ml of growth media. The dish is placed in a 37 °C, 5% $CO_2$ incubator for 24 h. After 1 day in culture, the tissue slices were subjected to immunohistochemical analysis.

### Statistical analysis

The results are expressed as mean ± SD from at least three separate experiments performed in triplicate. The differences between groups were determined with a two-tailed Student's *t*-test or ANOVA using GraphPad software. The results represent the mean ± SD of at least three independent experiments. Differences were considered statistically significant at $p < 0.05$. Statistically significant data are indicated by asterisks ($*p < 0.05$, $**p < 0.01$).

## Results

### Molecular characterization of CuS/tMDSC nanocarriers

The solvent dialysis method was used to prepare the self assembly of CuS/NorSun nano carriers encapsulating L-norvaline/sunitinib complexes (Fig. 1A). The PLGA-PEG was employed as it is an established biodegradable and biocompatible polymer approved by the FDA and is extensively used as a vehicle in the nano-delivery of chemotherapy drugs. Due to the amphiphilic nature of the polymer, it protects the interior CuS core from oxidative damage and thus enhancing the photothermal stability, and controlling the degradation rate of the nanocarriers *in vivo*. This mechanism enables prolonged blood circulation and effective accumulation in tumors through the enhanced permeability and retention effect. The resulting CuS/NorSun have a spherical structure and an average diameter of 85 nm as determined by dynamic light scattering (DLS) and AFM analysis (Fig. 1B and C). The solution of CuS/NorSun particles was stable in both PBS and 10% FBS with minor size difference for 72 h. This specific nanocarrier assembly method features high biocompatibility because L-norvaline/sunitinib complexes are highly chemically compatible with each other, guaranteeing increased biosafety and release both in *in vivo* and in *ex vivo* methodology (Fig. 1D). Using UV-vis spectroscopy, the optical characteristics of the CuS/NorSun NPs display a characteristic distinctive absorption peak at 960 nm (Fig. 1E). Transmission electron microscopy images confirmed the stable uniform spherical composition of the nanocarriers (Fig. 1F) whereas the fluorescence emission spectra is constant following incorporation of Rhodamine B (Fig. 1G). These observations highlight the importance of CuS/NorSun NCs as suitable candidates for delivering and releasing therapeutic agents at tumor tissues.

### Phototoxicity of CuS/NorSun nanocarriers

To further characterize CuS/NorSun antitumor profile, the phototoxicity of CuS/NorSun nanocarriers towards metastatic cells was evaluated. Highly aggressive metastatic cells H-1993 were incubated with various concentrations of CuS/NorSun nanocarriers. Cell viability of H-1993 decreased dramatically especially for concentration values above 2 mg $ml^{-1}$ which confirmed the eminent capability of ROS generation by CuS/NorSun nanocarriers (Fig. 2A). Next, the photothermal potential of NCs was further explored under normal and hypoxic pH values. Following incubation of H-1993 and A549 cells with NCs for 3 h, cells were irradiated with 970 nm laser (1 W $cm^{-2}$) for 10 min and then cell viability was assessed by CCK-8 assay. At normal pH, cell viability decreased significantly, while much higher cell viabilities could be observed at corresponding concentrations under hypoxic pH (Fig. 2B). Likewise, in A549 cells the acidic condition induces significantly higher cytotoxicity rates compared to H-1993 cells neutral and hypoxic pH (Fig. 2C). This behavior can be attributed to the CuS core of the NorSun nanocarriers, which is characterized by high phototoxicity as well as the production of highly toxic hydroxyl radicals (–OH) under acidic pH tumor microenvironment. Next, the photothermal capacity of the NCs was studied and in clinical perception using lung derived biopsy samples in order to evaluate immune responses. The 1 W $cm^{-2}$ intensity and 5 minutes exposure time period was chosen to avoid damage to normal cells. We used Ly6C and Ly6G antibodies in order to assess mMDSCs and gMDSCs levels, respectively (Fig. 2D). Ly6G/Ly6C positive cells were highly present in PBS-treated *ex vivo* tissue samples, and their expression was observed on the invasive edge in tumour samples. However, following treatment with NCs, Ly6G/Ly6C ratio was decreased dramatically, and only a minority of tumor cells were Ki67 positive and co-localized with the MDSCs (Fig. 2E–G). Similarly, NIR treatment on A459 cells showed an increase in the percentage of cells in the G0/G1phase and decrease in S and G2/M phases significantly following co-treatment compared to PBS group (Fig. 2H).

### Pharmacokinetics of intravenously injected CuS/MDSCs nanocarriers

To further exemplify the biochemical profile of CuS/NorSun NCs, a detailed pharmacokinetics study of the intravenously injected NCs was assessed to analyze their *in vivo* behavior. For that reason, biodistribution analysis of the nanocarriers in major organs on A549-xenograft-bearing mice treated was performed. Findings reveal elevated liver and spleen accumulation through the vascular-endothelial circulation (Fig. 3A). The concentration of CuS/MDSCs in blood at various time points post-injection was also evaluated. Blood circulation curve of the NCs in the blood of the A549 tumour-bearing C57BL/6 mice, shows a circulating half-life of 3.54 h in blood flow indicating the CuS/MDSCs enrichment in blood through the enhanced permeability and retention effect (Fig. 3B). Likewise, the eliminating rate constants of CuS/NorSun NCs were −0.420 and −0.019 μg $ml^{-1}$ per hour, for the first stage

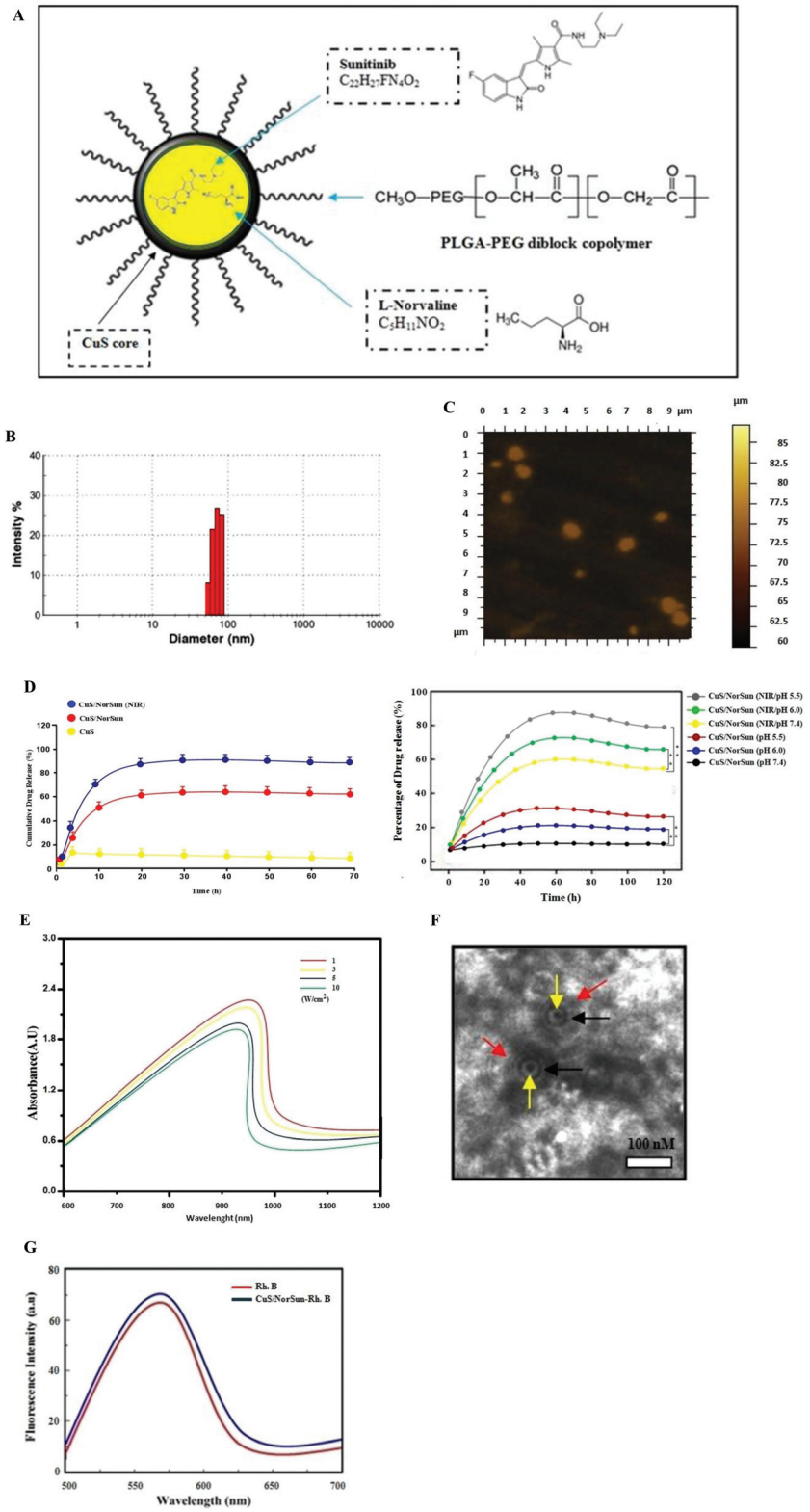


**Fig. 1** Characterization profile of CuS/NorSun nanosomes. (A) Schematic illustration of the CuS/NorSun NCs. (B) Size distribution analysis of CuS/NorSun NCs was examined by dynamic light scattering (DLS). (C) Representative atomic force microscopy (AFM) image of NCs. (D) Drug release curves under different pH conditions from CuS/NorSun NCs with or without NIR irradiation. (E) UV–vis absorbance spectra analysis. (F) Characteristic TEM image of the CuS/NorSun NCs (red arrow: PLGA-PEG, black: CuS core, yellow: norvaline/sunitinib drug complex). A clear dark CuS core can be seen within the nanocarriers. (G) The fluorescence emission spectra of CuS/NorSun NCs. The results represent the mean ± SD of three independent experiments. Differences were considered statistically significant at $p < 0.05$. Statistically significant data are indicated by asterisks (*$P < 0.05$, **$P < 0.01$).

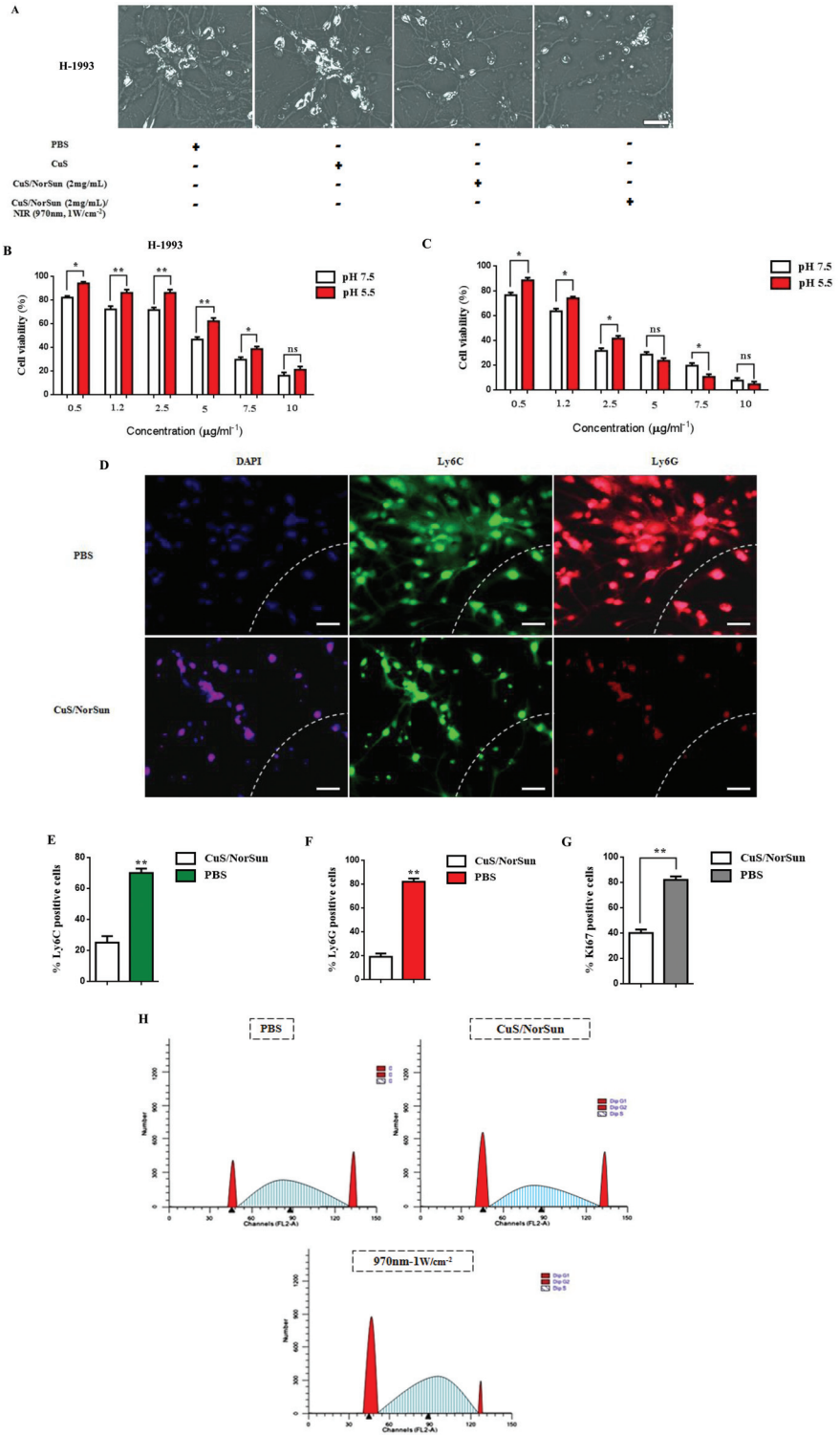


**Fig. 2** *In vitro* cytotoxicity profile of CuS/NorSun NCs. (A) Lung metastatic H-1993 cells were treated with CuS (4 mg $ml^{-1}$) or CuS/NorSun NCs (2 mg $ml^{-1}$) for 3 h, and then irradiation with 970 nm laser (1 W $cm^{-2}$) for 10 min. (B and C) Cytotoxicity evaluation of CuS/NorSun NCs in H-1993 and A549 cells under neutral or hypoxic pH. Cells were treated with CuS/NorSun NCs (0.5–10 μg $ml^{-1}$) for 3 h. Data represent the mean ± SD of three independent experiments (*$P$ < 0.05; **$P$ < 0.01). (D) Immunofluorescence analysis of Ly6C/Ly6G expression in lung biopsies (magnification ×200). Confocal microscopy image of Ly6C (green) and Ly6G labeled cells (red). Images were captured using Carl Zeiss fluorescence confocal microscope. (E–G) Expression levels Ly6C, Ly6G and Ki67 positive cells. Data represent the mean ± SD of three independent experiments (*$P$ < 0.05; **$P$ < 0.01). (H) Effect of CuS/NorSun NCs on cell cycle regulation. A549 cells were treated with NCs (4 mg $ml^{-1}$, 4 h) and subjected to FACS analysis. Following treatment, cells were collected and subjected to flow cytometric analysis of cell cycle distribution. Data represent the mean ± SD of three independent experiments (*$P$ < 0.05, **$P$ < 0.01).

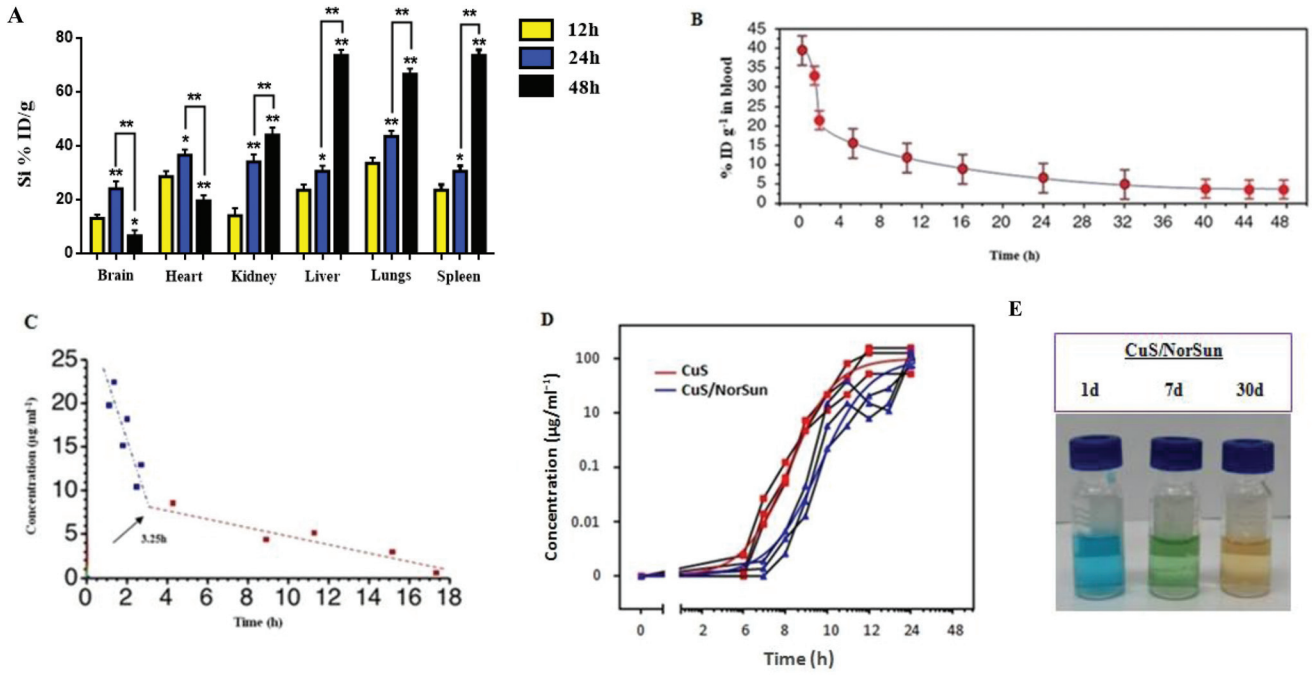


F

| Blood pharmacokinetics analysis of CuS/NorSun NCs. | | | | | |
|---|---|---|---|---|---|
| Groups | $T_{1/2}$ (h) | AUC (μg/h/ml) | Cmax (μg/ml) | CL (ml/h/kg) | Vd (ml/kg) |
| CuS/NorSun | 3.547 | 38.27 | 12.56 | 2.86 | 21.52 |
| Norvaline | 1.620 | 11.42 | 8.19 | 31.74 | 68.05 |

**Fig. 3** Pharmacokinetics and biodistribution analysis. (A) Quantitative biodistribution analysis of CuS/NorSun NCs in C57BL/6 mice by measuring the Cy5.5 fluorescence intensity in major organs at different time points post-injection. (B) Blood circulation curve of the intravenously injected CuS/NorSun NCs in C57BL/6 mice. (C) Eliminating rate curve of intravenously injected CuS/NorSun NCs according to the concentration (*C*) over time (*T*) relationship. (D) Quantitative concentration analysis of CuS and CuS/NorSun NCs in tumor area by measuring the Cy5.5 fluorescence intensity at different time points post-injection. (E) Stability of CuS/NorSun NCs after air exposure for 1–30 days. The NCs were dispersed in PBS and stored in room temperature for different periods of time. (F) Pharmacokinetic analysis of NCs in blood. The results represent the mean ± SD of three independent experiments. Differences were considered statistically significant at $p < 0.05$. Statistically significant data are indicated by asterisks (*$P$ < 0.05, **$P$ < 0.01).

and second stage respectively. The shifting time interval between the two stages was 3.25 h (Fig. 3C). On the contrary, elevated concentrations of NCs were found in the tumor area over 48 h in mice treated with CuS/NorSun and CuS NCs (Fig. 3D). This can be explained by the long-term biostability of the CuS/NorSun NCs in PBS, where they retain their maintain their rigidity and performance (Fig. 3E). Blood kinetics analysis in C57BL/6 mice reveals that CuS/NorSun NCs are detected in blood circulation for a significantly longer time compared with norvaline. Furthermore, NCs show increased area under curve (AUC), greater $T_{1/2}$ and $C_{max}$ against norvaline (Fig. 3F). However both clearance (CL) and volume of distribution ($V_d$) were significantly reduced over norvaline.

### Inhibition of MDSCs induction and tissue infiltration by metastatic tumor cells

To further investigate the therapeutic efficacy of CuS/NorSun and evaluate their activity *in vivo*, we employed A549 tumor xenograft model using C57BL/6 mice. CuS/NorSun NCs were administrated at different doses (5, 10 mg $kg^{-1}$) intratumorally in order to examine their therapeutic potential. Following tumor volume to 180–200 $mm^3$, mice received a single intratumoral (IT) injection of PBS, CuS and CuS/NorSun NCs. After tumor dissection, the comparison of results demonstrate that tumor growth was inhibited in CuS/NorSun treated mice compared with CuS and control group injected with PBS and mice body weight was not affected (Fig. 4A and B). An antitumor efficacy test was also performed using norvaline and/or sunitinib (ESI Fig. 1†). To further determine the effects of NCs inhibition on A549 tumor metastasis, an *in vivo* metastasis assay was employed. Findings show increased number lymph node metastatic foci in control group compared with CuS/NorSun-treated mice (Fig. 4C and D). In correlation with the increased expression of apoptotic proteins, the number of TUNEL positive cells was significantly increased by the treatment, suggesting that CuS/NorSun induces apoptosis (data not

 

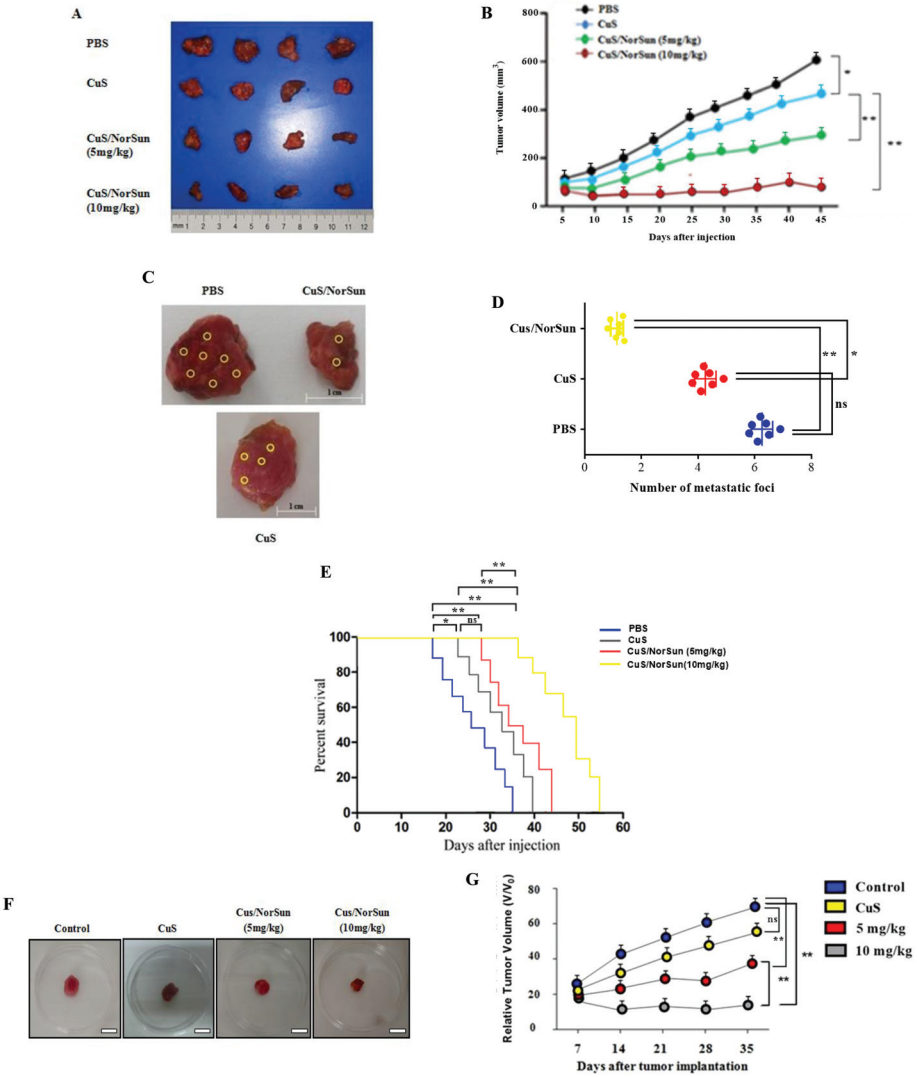


**Fig. 4** *In vivo* therapeutic efficacy of CuS/MDSCs NCs against A549 tumor xenografts. (A) Representative images of excised tumors from mice after treatment with CuS and CuS/MDSCs NCs (5–10 mg $kg^{-1}$) (B) Relative tumor volumes of A549 tumor bearing mice following treatment. (C) *In vivo* metastatic analysis of lymph node metastasis from control (PBS), CuS- and CuS/MDSCs NCs-treated groups. Images showed representative lymph node metastatic foci highlighted in yellow colour from different groups. (D) Statistical analysis of the number of metastatic foci of each group. (E) Survival rates of tumor-bearing mice after a 60 day tumor challenge in each group. Data were given as the mean ± SD ($n$ = 6). Mean values and error bars are defined as mean and SD respectively. (F) Representative photographs of excised tumors from mice after intravenous treatment with CuS and CuS/MDSCs NCs. (G) Relative tumor volumes ($V/V_0$) of A549 tumor bearing mice following intravenous administration. Data represent the mean ± SD of three independent experiments (*$P$ < 0.05; **$P$ < 0.01).

shown). Data reveal that mice administered with NCs show a slightly delayed tumor progression accompanied by high level of survival percentage. Moreover, survival analysis showed that in comparison with control and CuS groups, the CuS/NorSun-treated mice had long survival rate. Mice injected with CuS alone had a significantly shorter median overall survival after tumor implantation (approximately 37 days) than mice injected with CuS/NorSun NCs (median overall survival, 54 days) (Fig. 4E). To better comprehend the NCs tumor suppression efficacy, intravenous administration of NCs was performed in A549-tumor bearing mice. Findings based on relative tumor volume assessment exhibited significantly higher rates of tumor reduction for CuS/NorSun treatment compared to controls (Fig. 4F and G). Furthermore, tumor volume shrinkage and depleted Ki-67 antigen expression in NCs-treated groups could be also observed. Notably, the *in vivo* experiments indicated that the xenograft tumor was reduced by 57% after 14 days of treatment, and there was no recurrence, which further confirmed the potent therapeutic efficacy of the designed NCs.

### Activation of intratumoral immune responses *in vivo*

Given the effective *in vivo* circulation of CuS/NorSun nanocarriers, we assumed that these nanosomes can also stimulate

an effective intratumoral immune response. To support this hypothesis, we assessed immunological changes in the tumor microenvironment. Following administration of CuS/NorSun NCs in A549-tumor bearing mice, samples were collected and subjected to FACS analysis to evaluate immune responses. Findings show an upregulation of tumor infiltrating lymphocytes expression, especially for $CD8^+$ T cells by 27%, and $CD4^+$ T cells by 7% compared to PBS treatment (Fig. 5A). Furthermore, the presence of $CD161^+$ (NK1.1) cells reveals NK cell activation which subsequently enables antigen-specific T and B cell responses (Fig. 5B). Additionally, MDSC infiltration decreased considerably and MDSC subsets were characterized

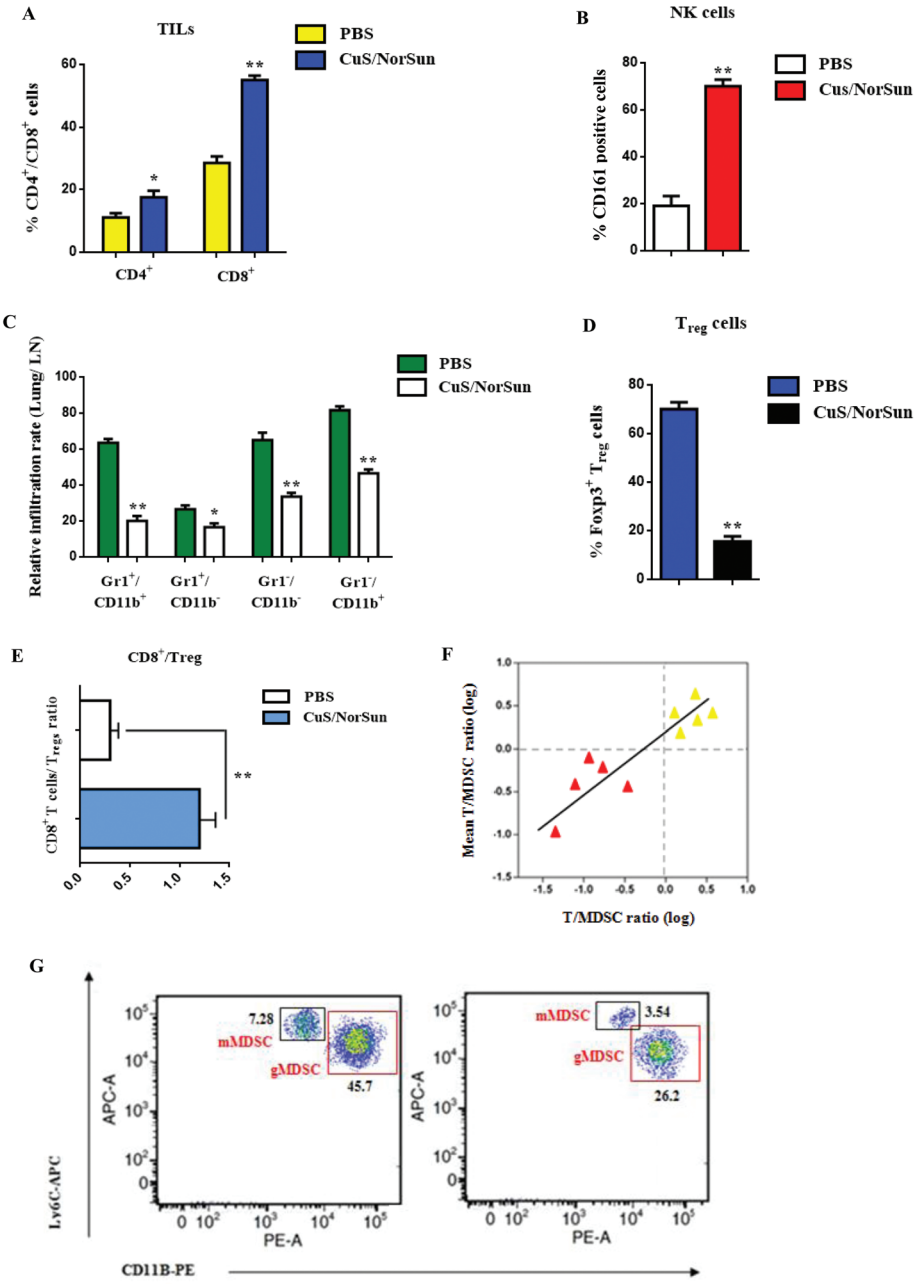


**Fig. 5** Assessment of intratumoral immune responses *in vivo*. (A) Expression levels of $CD4^+/CD8^+$ tumor infiltrating lymphocytes were evaluated by flow cytometry analysis. Both $CD4^+$ and $CD8^+$ T cells were isolated from PBMCs following centrifugation. (B) FACS assay of CD161 positive cells following PBS or CuS/MDSCs NCs treatment. (C) MDSC subset activation and expansion in immunocompetent C57BL/6 mice following administration of CuS/MDSCs NCs. MDSC infiltration was evaluated by the presence of gMDSC ($Gr^-/CD11b^-$) and mMDSC ($Gr^-/CD11b^+$) cells in primary tumors. The results represent the mean ± SD of three independent experiments. Differences were considered statistically significant at $p < 0.05$. (D) Percentage rate of $Foxp3^+$ T cells as analyzed by flow cytometry. (E) The relative ratio of $CD8^+$/Tregs among T cell population. (F) The mean T/MDSC cell ratio in tumor tissues following CuS/MDSCs NCs administration. (G) MDSC subset activation and expansion after treatment. MDSC infiltration was evaluated by the presence of gMDSC and mMDSC cells. Data represent the mean ± SD of three separate experiments (*$P < 0.05$; **$P < 0.01$).

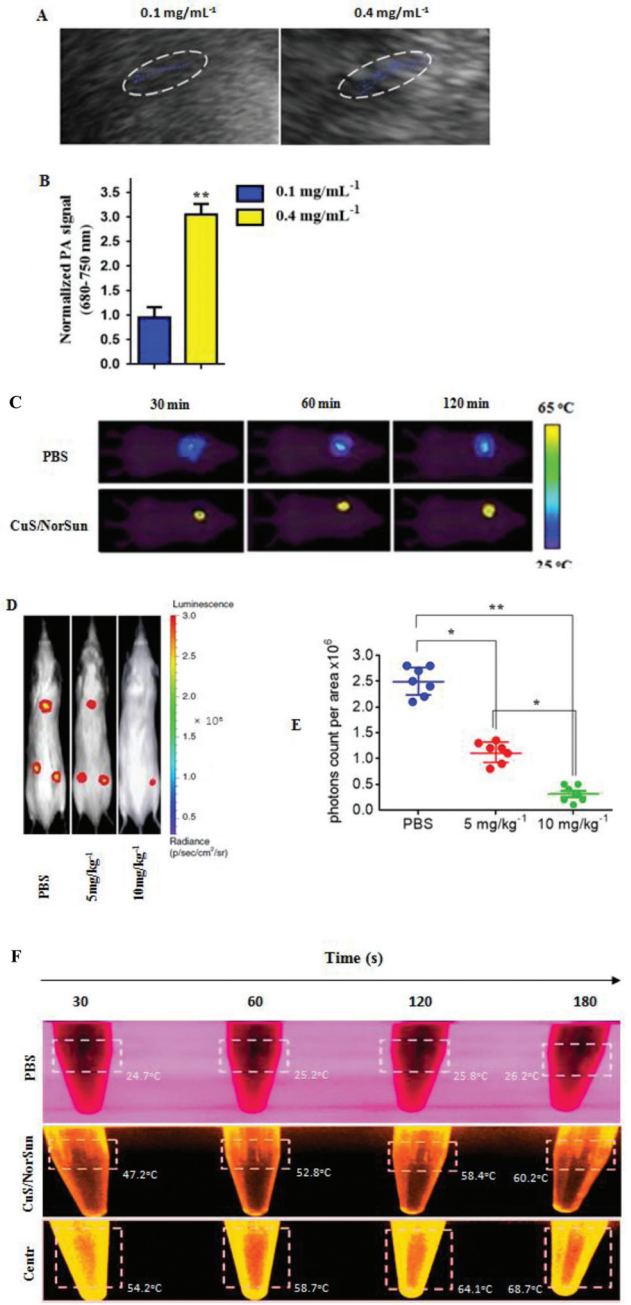


**Fig. 6** *In vivo* tumor imaging of CuS/NorSun nanocarriers. (A) Photoacoustic imaging of CuS/MDSCs NCs in PBS buffer with different concentrations (0.1, 0.4 mg $ml^{-1}$). (B) The relative intensity of the PA signal at 680–750 nm. (C) *In vivo* fluorescence images of the NCs-treated mice at different time points post-injection. (D) Bioluminescence imaging of mice from control (PBS) and CuS/MDSCs NCs-treated groups. (E) The bioluminescence values (photons per s per $cm^2$ per sr) were quantified for each group of mice and mean values ± SE were plotted. (F) Infrared thermal imaging of CuS/MDSCs NCs and PBS with NIR irradiation (980 nm, 1 W $cm^{-2}$). The results represent the mean ± SD of three independent experiments. Differences were considered statistically significant at $p < 0.05$. Statistically significant data are indicated by asterisks (*$P < 0.05$, **$P < 0.01$).

by the reduction of Gr/CD11b cell population in blood and tissue samples (Fig. 5C). Conversely, $Gr^+/CD11b^+$ levels were reduced by 42% following CuS/NorSun administration, whereas $Gr^-/Cd11b^-$ and $Gr^-/Cd11b^+$ expression declined by 28% and 35% respectively. MDSC downregulation by CuS/NorSun treatment also prompted Treg inhibition and increased intratumoral $CD8^+$/Treg ratio approximately four fold (Fig. 5D and E). Local T cell/MDSC balance is strongly associated with tumor recurrence and immune suppression. Following CuS/NorSun injection, T cell/MDSC ratio increased significantly after 24 h (Fig. 5F) which indicates systemic immune activation and immunosuppression reticence in tumor microenvironment. Subsequently, gMDSC and mMDSC expression levels were reduced by 19.5% and 37.4% respectively (Fig. 5G). Overall, MDSC-targeted NCs could efficiently deactivate MDSC-related tumor immunosuppression, thereby effectively preventing cancer recurrence and metastasis.

### *In vivo* tumor imaging of CuS/NorSun nanocarriers

To validate tumor-infiltration and systemic immune activation of TIL T cells, photoacoustic imaging was applied to further investigate the targeting ability of the NCs *in vivo*. Hence, dissimilar concentrations of CuS/Norsun nanosomes were intravenously injected into two groups of mice, respectively. PA signals at 970 nm were measured constantly and signal intensity was found to be amply dependent on CuS/Norsun concentration (Fig. 6A and B). To further visualize the biodistribution of the IV-injected nanocarriers. The localization of CuS NPs was monitored on A549-xenograft-bearing mice treated with 1054 nm laser (10 min) at the power of 1 W $cm^{-2}$ from 0.5 to 2 hours after the iv injection. We noticed that, as a result of the aggregation of CuS around the tumor a large proportion of the iv-injected CuS NPs was enriched in the tumor tissue through the enhanced permeability and retention effect (Fig. 6C). In addition, orthotopic growth of lung tumors of both the groups was monitored weekly by bioluminescence imaging. Bioluminescence imaging results revealed a significant decrease in the lung tumor volume of CuS/NorSun-treated mice compared to vehicle treated mice (Fig. 6D and E). The CuS/NorSun solution during NIR exposure at concentrations above 0.4 mg $mL^{-1}$, showed a rapid temperature raise from 18.4 °C to 60.2 °C in 180 s. Following one minute centrifugation, temperature was raised up to 67.7 °C and remained stable without compromising the photothermal efficiency (Fig. 6F). Notably, this is proof that the signal intensity is highly dependent on the concentration of CuS/NorSun solution. This perception has extensive potential for clinically translatable cancer theranostics in applications such as cancer diagnosis, treatment, or drug delivery.

## Discussion

MDSCs-mediated immunosuppression in metastatic carcinoma plays a critical role in tumor relapse and cancer cell chemoresistance.[25,26] Because MDSC are known to inhibit

T-cell sensitization to tumor antigens, their depletion may be clinically important for patient survival.[27,28] Our study demonstrated that MDSC immunosuppressive signaling can be restrained in both *in vivo* and *ex vivo* by using a CuS/NorSun photothermal nanocarrier model.[29] This biocompatible and biodegradable nanoplatform exhibits high levels of tumor-suppression efficacy towards A549 tumor xenograft mice both intratumorally and intravenously at similar dosages. The key advantage of this CuS-based nanotherapy approach is the simultaneous delivery to the tumor of two agents of different mechanisms of action. Furthermore copper sulfide NPs[30] have been known to possess exceptional characteristics, like low levels of biotoxicity, high photothermal conversion efficiency, unique molar extinction coefficient and superior NIR optical absorption.[31,32] Enclosement of norvaline and sunitinib in CuS NCs enables the photothermal ablation of tumors, without affecting the surrounding healthy tissues and prompts immune system re-activation. Moreover, norvaline (L-Nor) inhibits arginase activity[33] and can restrain inflammatory response *via* reducing S6K1, and oxidative stress levels.[34,35] Likewise, sunitinib blocks MDSC's action through inhibition of the tyrosine kinase activities of stem cell growth factor receptor (SCFR), PDGFR, VEGFR2 and other tyrosine kinases involved tumor progression and metastasis.[36,37] In summary, this study shows that the delivery of elaborately designed nanocatalysts into the tumor tissue can reverse tumor immunosuppression and reactivate the immune system's mechanisms. CuS/NorSun NCs have quicker release rates and show longer retention time in tumor tissues, likely due to their biochemical structure.[38–40] Overall, these findings demonstrate the crucial role of MDSC-targeted nanoplatform in inhibiting lung immunosuppressive metastasis and provide new opportunities for effective inhibition of metastatic neoplasia.

## Abbreviations

| | |
|---|---|
| MDSCs | Myeloid-derived suppressor cells |
| VEGF | Vascular endothelial growth factor |
| PDGF | Platelet-derived growth factor |
| NIR | Near infrared |
| PAI | Photoacoustic imaging |
| PTT | Photothermal therapy |
| FOXP3 | Forkhead box P3 |
| NSCLC | Non-small cell lung cancer |
| iNOS | Nitric oxide synthase |
| TKI | Tyrosine kinase inhibitor |
| Ly6G | Lymphocyte antigen 6 complex locus G6D |
| PLGA | Poly(lactic-*co*-glycolic acid) |
| PEG | Polyethylene glycol |
| Ly6C | Lymphocyte antigen 6 complex, locus C |
| TNF-α | Tumor necrosis factor alpha |
| mRCC | Metastatic renal cell carcinoma |
| SCFR | Stem cell growth factor receptor |
| TILs | Tumor infiltrating lymphocyte |

## Author contributions

D. A., S. P., K. D., conceived and planned the experiments. D. A., S. P., K. D., and P. Z., carried out the experiments. S. P., C. B., and K. P., acquired and analyze data, and managed patients. P. Z., S. P., L. F., and K. Z., contributed to sample preparation. S. P., K. D., D. A., and K. Z., contributed to the interpretation of the results. T. K., and W. H.-S., took the lead in writing the manuscript. All authors provided critical feedback and helped shape the research, analysis and manuscript.

## Funding

This work was funded by grant (grant number: GRC-70/1216) from the Research Committee of Aristotle University of Thessaloniki.

## Conflicts of interest

The authors declare no conflict of interest.

## Acknowledgements

The author would like to thank Professor Konstantinos Zarogoulidis for reading the manuscript and providing comments and advice.

## References

1 P. Beckett, L. J. Tata and R. B. Hubbard, Risk factors and survival outcome for non-elective referral in non-small cell lung cancer patients analysis based on the National Lung Cancer Audit, *Lung Cancer*, 2014, **83**, 396–400.
2 L. T. Tanoue, N. T. Tanner, M. K. Gould and G. A. Silvestri, Lung cancer screening, *Am. J. Respir. Crit. Care Med.*, 2015, **191**, 19–33.
3 P. Khanna, N. Blais, P. O. Gaudreau and L. Corrales-Rodriguez, Immunotherapy Comes of Age in Lung Cancer, *Clin. Lung Cancer*, 2017, **18**(1), 13–22.
4 F. R. Hirsch, G. V. Scagliotti, J. L. Mulshine, R. Kwon, W. J. Curran Jr., Y. L. Wu and L. Paz-Ares, Lung cancer: current therapies and new targeted treatments, *Lancet*, 2017, **389**(10066), 299–311.
5 R. Sackstein, T. Schatton and S. R. Barthel, T-lymphocyte homing: an underappreciated yet critical hurdle for successful cancer immunotherapy, *Lab. Invest.*, 2017, **97**(6), 669–697.
6 M. W. Teng, S. F. Ngiow, A. Ribas and M. J. Smyth, Classifying Cancers Based on T- cell Infiltration and PD-L1, *Cancer Res.*, 2015, **75**(11), 2139–2145.

 

7 P. J. Stambrook, J. Maher and F. Farzaneh, Cancer Immunotherapy: Whence and Whither, *Mol. Cancer Res.*, 2017, **15**(6), 635–650.
8 A. Makkouk and G. J. Weiner, Cancer immunotherapy and breaking immune tolerance: new approaches to an old challenge, *Cancer Res.*, 2015, **75**(1), 5–10.
9 V. Bronte, S. Brandau, S. H. Chen, M. P. Colombo, A. B. Frey, T. F. Greten, S. Mandruzzato, P. J. Murray, A. Ochoa, S. Ostrand-Rosenberg, P. C. Rodriguez, A. Sica, V. Umansky, R. H. Vonderheide and D. I. Gabrilovich, Recommendations for myeloid-derived suppressor cell nomenclature and characterization standards, *Nat. Commun.*, 2016, **7**, 12150.
10 F. Veglia, M. Perego and D. Gabrilovich, Myeloid-derived suppressor cells coming of age, *Nat. Immunol.*, 2018, **19**(2), 108–119.
11 P. Qu, L. Z. Wang and P. C. Lin, Expansion and functions of myeloid-derived suppressor cells in the tumor microenvironment, *Cancer Lett.*, 2016, **380**(1), 253–256.
12 Z. Deng, Y. Rong, Y. Teng, X. Zhuang, A. Samykutty, J. Mu, L. Zhang, P. Cao, J. Yan, D. Miller and H. G. Zhang, Exosomes miR-126a released from MDSC induced by DOX treatment promotes lung metastasis, *Oncogene*, 2017, **36**(5), 639–651.
13 A. R. Pyzer, L. Cole, J. Rosenblatt and D. E. Avigan, Myeloid-derived suppressor cells as effectors of immune suppression in cancer, *Int. J. Cancer*, 2016, **139**(9), 1915–1926.
14 S. Ostrand-Rosenberg, P. Sinha, D. W. Beury and V. K. Clements, Cross-talk between myeloid- derived suppressor cells (MDSC), macrophages, and dendritic cells enhances tumor- induced immune suppression, *Semin. Cancer Biol.*, 2012, **22**(4), 275–281.
15 J. A. Chesney, R. A. Mitchell and K. Yaddanapudi, Myeloid-derived suppressor cells-a new therapeutic target to overcome resistance to cancerimmunotherapy, *J. Leukocyte Biol.*, 2017, **102**(3), 727–740.
16 F. De Sanctis, S. Solito, S. Ugel, B. Molon, V. Bronte and I. Marigo, MDSCs in cancer: Conceiving new prognostic and therapeutic targets, *Biochim. Biophys. Acta*, 2016, **1865**(1), 35–48.
17 P. Venkatesan, Intermittent sunitinib for metastatic renal cell carcinoma, *Lancet Oncol.*, 2017, **18**(3), e139.
18 J. W. Wragg, V. L. Heath and R. Bicknell, Sunitinib Treatment Enhances Metastasis of Innately Drug-Resistant Breast Tumors, *Cancer Res.*, 2017, **77**(4), 1008–1020.
19 O. Draghiciu, H. W. Nijman, B. N. Hoogeboom, T. Meijerhof and T. Daemen, Sunitinib depletes myeloid-derived suppressor cells and synergizes with a cancer vaccine to enhance antigen-specific immune responses and tumor eradication, *OncoImmunology*, 2015, **4**(3), e989764.
20 Q. Zhao, J. Guo, G. Wang, Y. Chu and X. Hu, Suppression of immune regulatory cells with combined therapy of celecoxib and sunitinib in renal cell carcinoma, *Oncotarget*, 2017, **8**(1), 1668–1677.
21 L. Gao, J. H. Zhang, X. X. Chen, H. L. Ren, X. L. Feng, J. L. Wang and J. H. Xiao, Combination of L- Arginine and L-Norvaline protects against pulmonary fibrosis progression induced by bleomycin in mice, *Biomed. Pharmacother.*, 2019, **113**, 108768.
22 Q. Q. Ji, Z. P. Fang, Q. Ye, C. W. Chi and E. D. Wang, Self-protective responses to norvaline- induced stress in a leucyl-tRNA synthetase editing-deficient yeast strain, *Nucleic Acids Res.*, 2017, **45**(12), 7367–7381.
23 P. Zarogoulidis, S. Petanidis, K. Domvri, E. Kioseoglou, D. Anestakis, L. Freitag, *et al.*, Autophagy inhibition upregulates $CD4^+$ tumor infiltrating lymphocyte expression via miR-155 regulation and TRAIL activation, *Mol. Oncol.*, 2016, **10**, 1516–1531.
24 K. Leithner, C. Wohlkoenig, E. Stacher, J. Lindenmann, N. A. Hofmann, B. Gallé, *et al.*, Hypoxia increases membrane metallo-endopeptidase expression in a novel lung cancer ex vivo model - role of tumor stroma cells, *BMC Cancer*, 2014, **14**, 40.
25 V. Fleming, X. Hu, R. Weber, V. Nagibin, C. Groth, P. Altevogt, J. Utikal and V. Umansky, Targeting Myeloid-Derived Suppressor Cells to Bypass Tumor-Induced Immunosuppression, *Front. Immunol.*, 2018, **9**, 398.
26 A. A. Wu, V. Drake, H. S. Huang, S. Chiu and L. Zheng, Reprogramming the tumor microenvironment: tumor-induced immunosuppressive factors paralyze T cells, *OncoImmunology*, 2015, **4**(7), e1016700.
27 C. R. Lee, Y. Kwak, T. Yang, J. H. Han, S. H. Park, M. B. Ye, W. Lee, K. Y. Sim, J. A. Kang, Y. C. Kim, S. K. Mazmanian and S. G. Park, Myeloid-Derived Suppressor Cells Are Controlled by Regulatory T Cells via TGF-β during Murine Colitis, *Cell Rep.*, 2016, **17**(12), 3219–3232.
28 T. A. Barnes and E. Amir, HYPE or HOPE: the prognostic value of infiltrating immune cells in cancer, *Br. J. Cancer*, 2017, **117**(4), 451–460.
29 A. I. Papadakis, C. Sun, T. A. Knijnenburg, Y. Xue, W. Grernrum, M. Hölzel, *et al.*, SMARCE1 suppresses EGFR expression and controls responses to MET and ALK inhibitors in lung cancer, *Cell Res.*, 2015, **25**, 445–458.
30 S. Goel, F. Chen and W. Cai, Synthesis and biomedical applications of copper sulfide nanoparticles: from sensors to theranostics, *Small*, 2014, **10**(4), 631–645.
31 S. Wang, A. Riedinger, H. Li, C. Fu, H. Liu, L. Li, T. Liu, L. Tan, M. J. Barthel, G. Pugliese, F. De Donato, M. S. D'Abbusco, X. Meng, L. Manna, H. Meng and T. Pellegrino, Plasmonic copper sulfide nanocrystals exhibiting near-infrared photothermal and photodynamic therapeutic effects, *ACS Nano*, 2015, **9**(2), 1788–1800.
32 N. Li, Q. Sun, Z. Yu, X. Gao, W. Pan, X. Wan and B. Tang, Nuclear-Targeted Photothermal Therapy Prevents Cancer Recurrence with Near-Infrared Triggered Copper Sulfide Nanoparticles, *ACS Nano*, 2018, **12**(6), 5197–5206.
33 C. I. Chang, J. C. Liao and L. Kuo, Macrophage arginase promotes tumor cell growth and suppresses nitric oxide-mediated tumor cytotoxicity, *Cancer Res.*, 2001, **61**(3), 1100–1106.

34 A. De, M. F. Singh, V. Singh, V. Ram and S. Bisht, Treatment effect of l-Norvaline on the sexual performance of male rats with streptozotocin induced diabetes, *Eur. J. Pharmacol.*, 2016, **771**, 247–254.

35 B. Polis, K. D. Srikanth, E. Elliott, H. Gil-Henn and A. O. Samson, L-Norvaline Reverses Cognitive Decline and, Synaptic Loss in a Murine Model of Alzheimer's Disease, *Neurotherapeutics*, 2018, **15**(4), 1036–1054.

36 K. S. Gajiwala, J. C. Wu, J. Christensen, G. D. Deshmukh, W. Diehl, J. P. DiNitto, J. M. English, M. J. Greig, Y. A. He, S. L. Jacques, E. A. Lunney, M. McTigue, D. Molina, T. Quenzer, P. A. Wells, X. Yu, Y. Zhang, A. Zou, M. R. Emmett, A. G. Marshall, H. M. Zhang and G. D. Demetri, KIT kinase mutants show unique mechanisms of drug resistance to imatinib and sunitinib in gastrointestinal stromal tumor patients, *Proc. Natl. Acad. Sci. U. S. A.*, 2009, **106**(5), 1542–1547.

37 W. Zhai, S. Li, J. Zhang, Y. Chen, J. Ma, W. Kong, D. Gong, J. Zheng, W. Xue and Y. Xu, Sunitinib-suppressed miR-452-5p facilitates renal cancer cell invasion and metastasis through modulating SMAD4/SMAD7 signals, *Mol. Cancer*, 2018, **17**(1), 157.

38 S. Goel, F. Chen and W. Cai, Synthesis and biomedical applications of copper sulfide nanoparticles: from sensors to theranostics, *Small*, 2014, **10**(4), 631–645.

39 O. Rubilar, M. Rai, G. Tortella, M. C. Diez, A. B. Seabra and N. Durán, Biogenic nanoparticles: copper, copper oxides, copper sulphides, complex coppernanostructures and their applications, *Biotechnol. Lett.*, 2013, **35**(9), 1365–1375.

40 M. Tamada, O. Nagano, S. Tateyama, M. Ohmura, T. Yae, T. Ishimoto, *et al.*, Modulation of glucose metabolism by CD44 contributes to antioxidant status and drug resistance in cancer cells, *Cancer Res.*, 2012, **72**, 1438–1448.